ChemComm

COMMUNICATION

View Article Online
View Journal

Cite this: DOI: 10.1039/d5cc04653j

Received 18th August 2025,
Accepted 9th September 2025

DOI: 10.1039/d5cc04653j

rsc.li/chemcomm

Carbonic anhydrase-IX targeted copper-doped carbon dots as a theranostic probe for treating triple negative breast cancer

Aftab Hossain Khan, Sudeshna Pal and Prasanta Kumar Das *

Herein, we demonstrate selective diagnosis and chemodynamic therapy in triple negative breast cancer (TNBC) cells by carbonic anhydrase-IX targeted acetazolamide-functionalized copper-doped carbon dots (CuCD-Az). CuCD-Az showed ~3-fold higher cytotoxicity to TNBC compared to normal cells by ROS-mediated apoptosis *via* Fenton-like reaction.

Breast cancer is a major global health challenge, mostly diagnosed in females and accounting for approximately 25% of cancer cases. Triple-negative breast cancer (TNBC), which represents ~15–20% of cases, designates a distinct subtype of breast cancer characterized by the absence of oestrogen receptors (ER), progesterone receptors (PR), and human epidermal growth factor receptor 2 (HER2) expression.[1] Despite significant progress in breast cancer survival rates, conventional chemotherapy and radiotherapy suffer from severe side effects and lack of target specificity.

In this context, target specific diagnostic probes with therapeutic potential offer a promising strategy to enhance the efficacy of cancer treatment. Several drug delivery vehicles such as liposomes, hydrogels, dendrimers, carbon nanotubes, nanoparticle-based theranostics *etc.* have been explored for targeted cancer therapy, each with benefits and limitations.[2–4] In the recent past, carbon dots with intrinsic fluorescence, photostability and biocompatibility have made remarkable contributions in therapeutics, sensing, bioimaging, drug delivery, and others.[5–8] Carbon dots hold strong potential to serve as theranostic tools due to their easy synthesis and tailor-made surface functionalization.[9] Alongside this, the drawbacks of conventional therapies, such as drug resistance and tumour recurrence, have escalated the need for new strategies for treating cancer. To this end, chemodynamic therapy (CDT), a term proposed by Bu *et al.* in 2016, has gained significant attention as an alternative therapeutic strategy.[10] CDT utilizes Fenton or Fenton-like reactions to convert intracellular H_2O_2 into reactive oxygen species (ROS), thereby inducing apoptosis in cancer cells.[11] The efficiency of ROS-based therapies is restricted by a vital intracellular antioxidant, glutathione (GSH), which maintains the redox homeostasis in cells and protects them from the effect of ROS.[12,13] Cancer cells contain a higher concentration of GSH that neutralizes a substantial amount of ROS, resulting in lower efficacy of CDT. Therefore, a significant amount of ROS generation along with the depletion of GSH is required for improvement in CDT.[13] In this context, the Cu^{2+} ion plays a key role in converting GSH to GSSG and gets reduced to Cu^{+} ion, which reacts with H_2O_2 to produce ROS *via* Fenton-like reaction and the plummeted level of GSH leads to the accumulation of ROS.[14,15] Therefore, Cu^{2+}-ion based CDT agents are gaining notable attention. To date, several CDT agents have been studied, such as dual cation-containing Zn nitroprusside, CsMnP metal organic frameworks (MOFs), Cu^{2+}–pyropheophorbide a–cystine conjugate, cancer cell-coated copper sulfide nanoparticles *etc.* (Table S1). Glucose oxidase-loaded nanocarriers alone or in combination with metal ions (GOD encapsulated Cu doped ZIFs) have also played a significant role in CDT.[16] However, the complex synthetic procedures and stability issues restrict the clinical applicability of these CDT agents. In this regard, copper-doped carbon dots can be a potential CDT agent due to their intrinsic characteristics. Despite these advantages, reports on Cu–CDs in CDT remain scarce, highlighting a promising route to be explored in cancer therapy.

Targeted therapies focusing on tumor biomarkers offer promise for early detection, prognosis, and selective treatment of TNBC. Carbonic anhydrase-IX (CA-IX), a Zn containing metalloenzyme, is one such biomarker.[17] CA-IX, one of the 15 human isoenzymes of the α-carbonic anhydrase family, is a tumour-associated transmembrane protein that is involved in the regulation of intracellular CO_2 levels. CA-IX facilitates reversible hydration of CO_2 producing proton (H^+) and bicarbonate ions (HCO_3^-), which balances intracellular as well as extracellular pH levels to promote tumour cell survival and enhance migratory potential.[18] CA-IX can be a potential biomarker for targeted therapy because of its overexpression in aggressive breast cancer in comparison to normal tissues.[18] Therefore, copper-doped carbon dots with a CA-IX targeting motif could be a novel theranostic agent for improved cancer treatment

School of Biological Sciences, Indian Association for the Cultivation of Science, Jadavpur, Kolkata-700032, India. E-mail: bcpkd@iacs.res.in

through CDT. To date, there are very few reports on Cu^{2+}-based nanocatalysts, and Cu(II)–BODIPY photosensitizers for combination and photodynamic therapy with the assistance of a CA-IX targeted inhibitor. Some additional attempts were made using CA-IX targeting nanovesicles, silica/iron nanoparticles and small molecule drug conjugates for cancer treatment.[19–25] However, currently there is almost no report on CA-IX targeted Cu^{2+} ion-doped carbon dots as theranostic probes. Keeping this in mind, we aimed to develop CA-IX targeted copper-doped carbon dots as a target specific theranostic probe for treating TNBC *via* CDT.

In order to synthesize CA-IX targeted carbon dots, carboxyl rich surface-functionalized carbon dots (**CD**) were prepared from citric acid and diethylenetriamine (1 : 0.3 mol ratio) *via* hydrothermal method.[26] Copper-doped carbon dots (**CuCD**) were prepared from citric acid, diethylenetriamine and copper nitrate (1 : 0.3 : 0.5 mol ratio) through optimization following the similar protocol. Both carbon dots were surface-modified with the hydrolysed product of acetazolamide (**CD-Az** and **CuCD-Az**, Fig. 1a, c and Fig. S1, S2) *via* EDC-NHS coupling (Scheme S1 and S2) to make it CA-IX target specific. Acetazolamide is a sulfonamide-derived CA-IX inhibitor capable of binding with the active zinc centre of CA-IX.[17] The size of **CD-Az** and **CuCD-Az** was around ~3–5 nm as determined from the respective TEM and AFM images (Fig. 1b, d and Fig. S3). The ζ-potential of the carbon dots was found to be −0.65 mV for **CD-Az** and +0.61 mV for **CuCD-Az**. According to the UV-vis spectra, the absorbance maxima of **CD** and **CD-Az** were at 350 nm, while the same for copper-doped carbon dots (**CuCD** and **CuCD-Az**) got slightly shifted to 345 nm (Fig. 2a) due to copper doping. Additionally, a shoulder peak was observed at around 275–280 nm for both **CD-Az** and **CuCD-Az**, which accounted for the carbon dot surface tethered acetazolamide moiety having absorbance in a similar range (Fig. 2a). Therefore, the UV-vis spectra confirmed the successful functionalization of the carbon dots with acetazolamide. Both carbon dots showed blue fluorescence in the visible region under UV torch irradiation (excitation at 365 nm, Fig. 2b and Fig. S4). The emission maxima for **CD-Az** and **CuCD-Az** were observed at λ_{em} = ~455 nm and ~460 nm, respectively upon excitation at λ_{ex} = 350 nm (Fig. 2b and Fig. S4). According to the excitation dependent emission, both carbon dots showed emission maxima at λ_{em} = ~460 nm and ~465 nm for **CD-Az** and **CuCD-Az**, respectively, upon excitation at λ_{ex} = 370 nm (Fig. 2b and Fig. S4). The quantum yields of **CD-Az** and **CuCD-Az** were found to be 6% and 5% with respect to the quinine sulfate.

To ascertain the successful copper doping as well as surface functionalization with acetazolamide, XPS analysis was performed for both CDs. The XPS spectra of **CuCD** and **CuCD-Az** showed peaks at 284 eV, 400 eV and 530 eV that denoted C(1s), N(1s) and

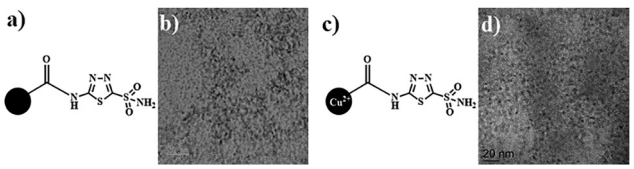

Fig. 1 (a) Structure and (b) TEM image of carbon dot **CD-Az** and (c) structure and (d) TEM image of carbon dot **CuCD-Az**.

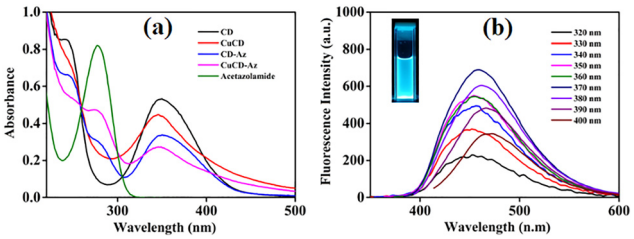

Fig. 2 (a) UV-vis spectra of the carbon dots and acetazolamide and (b) excitation dependent emission spectra of **CD-Az**. Inset: image of blue fluorescence of carbon dots under UV torch irradiation.

O(1s) orbitals (Fig. S5a and c). Moreover, two peaks were observed at 931 eV and 951 eV corresponding to Cu $2p_{3/2}$ and Cu $2p_{1/2}$ in the high resolution XPS spectra of both the carbon dots (Fig. S5b and d), which confirmed the successful doping of Cu^{2+}. Another peak in the XPS spectra of **CuCD-Az** was observed at 163 eV, denoting S 2p (Fig. S5a), which was absent in the XPS spectra of **CuCD**, and ensured the successful functionalization of the carbon dots with acetazolamide. Furthermore, the XPS spectrum analysis of **CuCD-Az** confirmed that **CuCD-Az** contained C (48%), N (13%), O (35%), Cu (2%) and S (2%) whereas **CuCD** contained C (47%), N (8%), O (41%) and Cu (4%). The presence of sulphur in **CD-Az** was confirmed from EDX data ensuring the existence of an acetazolamide moiety (Fig. S6). FTIR study of **CD-Az** and **CuCD-Az** showed two sharp peaks at ~1180 cm^{-1} and ~1350 cm^{-1} due to the symmetric stretching and asymmetric stretching of S=O bonds in sulfonamides, which is also present in the FTIR spectra of acetazolamide (Fig. S7). Similarly, two sharp peaks at ~585 cm^{-1} and 650 cm^{-1}, were observed in the fingerprint region of both **CD-Az** and **CuCD-Az**. Thus, the IR spectra supported the presence of acetazolamide on the surface of both the carbon dots. Also, a peak ranging from 20° to 30° in the XRD spectra (Fig. S8) confirmed the amorphous nature of **CD-Az** and **CuCD-Az**.

Next, the chemodynamic function of **CuCD-Az** was tested upon reaction with GSH. The efficacy of CDT is hindered by a natural antioxidant, GSH, which is present in a high concentration in cancer cells and degrades the accumulated ROS to maintain optimal oxidative stress. Cu^{2+} ion is capable of oxidizing GSH into GSSG, that results in the depletion of GSH concentration. Here, the GSH depletion ability of **CuCD-Az** was studied using DTNB (5,5′-dithiobis-2-nitrobenzoic acid) as a probe. DTNB has an absorbance maxima at ~325 nm. GSH reacts with DTNB producing 5-mercapto 2-nitrobenzoic acid (TNB), which is yellow in colour and absorbs at ~410 nm (Scheme S3). The Cu^{2+} ion converts GSH into GSSG, which is unable to react with DTNB and as a result, the absorbance peak for TNB at 410 nm decreases (Fig. 3). Here, with increasing concentration of **CuCD-Az** (20–200 μg mL^{-1}), the intensity of the absorbance peak for TNB at ~410 nm steadily decreased, while the absorbance peak intensity for DTNB at ~325 nm gradually increased. Cu^{2+} in **CuCD-Az** converted GSH into GSSG leading to the inefficient conversion of DTNB to TNB due to the depleted level of GSH. Notably, at 200 μg mL^{-1} of **CuCD-Az**, almost all GSH was converted to GSSG by Cu^{2+} ions as no peak of TNB was observed and only the significant presence of unreacted DTNB was noted (Fig. 3). This ensured the potential candidature of **CuCD-Az** in CDT.

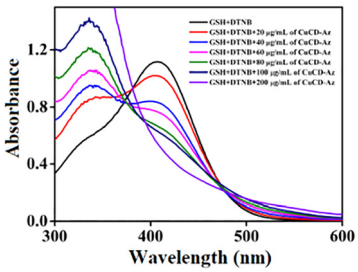

Fig. 3 DTNB UV-vis study for GSH depletion using **CuCD-Az**.

Next, we investigated the ability of the acetazolamide-functionalized carbon dots (**CD-Az**) to selectively target triple negative breast cancer cells over normal cells. Prior to that, the endogenous expression of CA-IX in TNBC, MDA-MB-231 and 4T1 cell lines was confirmed from western blot analysis (Fig. 4a, b, raw data, Fig. S9). The selective uptake of **CD-Az** in comparison to the non-functionalized **CD** by cancer cells was also assessed from CA-IX expression (Fig. 4a and b). In the case of **CD-Az** treated MDA-MB-231 and 4T1 cells, the expression of CA-IX decreased, whereas for non-functionalized **CD** treated cells, the expression of CA-IX remained unaltered in comparison to that in untreated cells (Fig. 4a and b). The reduced CA-IX expressions in TNBC cells depict the target-specific successful binding of acetazolamide-functionalized carbon dots on the surface of the respective cancer cells. Next, the intrinsic fluorescence of the carbon dots was utilized for selective bioimaging of cancer cells. Fluorescence microscopy revealed the bright blue fluorescence for both MDA-MB-231 and 4T1 cells treated with **CD-Az** (Fig. 4c and f). On the other hand, faint blue fluorescence was observed in HEK-293 and NIH3T3 cells when treated with **CD-Az** (Fig. 4i and l). In contrast, when the cells were treated with non-functionalized **CD**, comparable blue fluorescence was observed in all four cell lines (Fig. S10a–h). It ensured the lack of target specificity of the carbon dots without an acetazolamide moiety. The CA-IX specificity of **CD-Az** was further confirmed by blocking experiments in 4T1 and MDA-MB-231 cells. Very faint blue fluorescence was observed in both acetazolamide pre-treated 4T1 and MDA-MB-231 cells (Fig. S11) in comparison to untreated cells (Fig. 4c and f). Binding of an acetazolamide moiety to CA-IX prevented it from conjugating with **CD-Az** resulting in the failure of **CD-Az** internalization into cancer cells. This further confirmed that the selective internalization of **CD-Az** in TNBC took place through the interaction between CA-IX and the acetazolamide moiety. To further support the target specificity of **CD-Az** towards cancer cells, flow cytometric analysis was performed for all four cell lines treated with **CD-Az**. For MDA-MB-231 and 4T1 cells, significantly high mean fluorescence intensity values of ~33 600 and ~48 100 were observed, respectively, whereas for HEK-293 and NIH3T3 cells, they were considerably low at ~11 500 and ~12 000 (Fig. 4e, h, k and n, Fig. S12). According to flow cytometry data, ~3–4-fold selectivity of **CD-Az** towards TNBC cells was observed in comparison to HEK-293 and NIH3T3 cells (Fig. S12). This is due to the binding of the acetazolamide moiety of **CD-Az** with over-expressed CA-IX enzyme in TNBC cells leading to bright blue fluorescence inside the cells, while feeble blue fluorescence was observed in non-cancerous cells due to the unavailability of the

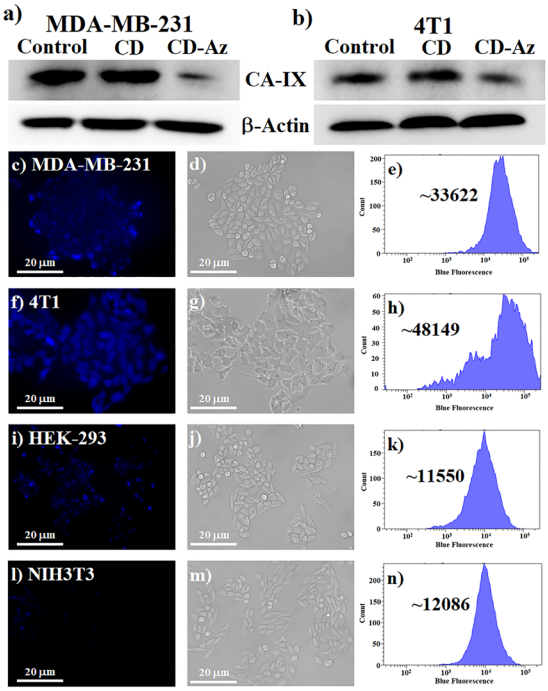

Fig. 4 Immunoblot analysis of carbonic anhydrase-IX levels in (a) MDA-MB-231 and (b) 4T1 treated with **CD** and **CD-Az** for 24 h. β-actin levels are shown as a loading control. Fluorescence microscopic images, brightfield images and corresponding flow cytometric analysis plots of **CD-Az** treated (c)–(e) MDA-MB-231, (f)–(h) 4T1, (i)–(k) HEK-293 and (l)–(n) NIH3T3 cells. Scale bars correspond to 20 μm. Mean fluorescence intensity values are mentioned in the insets.

CA-IX enzyme. All these experiments ascertained that the target specificity of **CD-Az** toward selective diagnosis of TNBC cells was achieved due to the presence of the acetazolamide moiety.

After ensuring the target specificity of **CD-Az**, we have explored the selective cytotoxicity of **CuCD-Az** *via* CDT. As mentioned, in the presence of GSH, Cu^{2+} gets reduced to Cu^{+}, which upon reaction with intracellular H_2O_2 produces ROS that induces apoptosis in cancer cells. Alongside this, the efficacy of CDT may also increase due to the reduced level of GSH that neutralizes ROS. MTT assay showed that both **CD** and **CD-Az** exhibited ~80% cell viability for up to 3 mg mL^{-1} (Fig. S13) after 24 h of incubation in all four cell lines ensuring their notable biocompatibility. Furthermore, the hemocompatibility of **CuCD-Az** was evaluated, which showed dose-dependent hemolysis of RBCs maximum up to ~35% at the highest concentration of **CuCD-Az** (3 mg mL^{-1}, Fig. S14) confirming minimal toxicity and potential biocompatibility of **CuCD-Az**. In case of both **CuCD** and **CuCD-Az**, the cytotoxicity got steadily enhanced from ~10% at 50 μg mL^{-1} to ~90% at 3 mg mL^{-1} for 4T1 cells (Fig. 5a and b). A similar trend was observed for MDA-MB-231 cells, where both **CuCD** and **CuCD-Az** induced ~5% killing at 50 μg mL^{-1}, which increased to ~85% at the highest concentration of carbon dots (3 mg mL^{-1}). Higher cytotoxicity of **CuCD** and **CuCD-Az** in cancer cells arises due to the enhanced CDT by means of efficient conversion of Cu^{2+} to Cu^{+} by overexpressed GSH and subsequent Fenton-like reaction with abundant H_2O_2 that led to the generation of a greater amount of ROS. Notably, **CuCD** exhibited ~55% and ~65% killing in normal

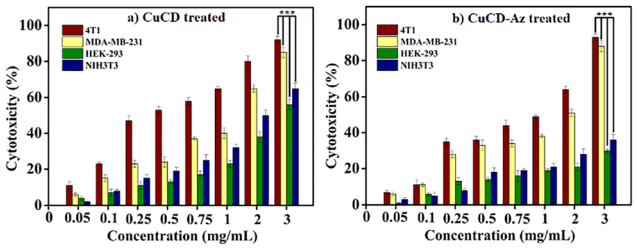

Fig. 5 Cytotoxicity of (a) **CuCD** and (b) **CuCD-Az** in 4T1, MDA-MB-231, HEK-293 and NIH3T3 cells determined by MTT assay. Values are expressed as mean ± SEM from three independent experiments. ***$p < 0.001$ *vs.* **CuCD** and ***$p < 0.001$ vs **CuCD-Az** treated 4T1, MDA-MB-231 HEK-293, and NIH3T3 cells.

HEK-293 and NIH3T3 cells, respectively, while **CuCD-Az** exhibited only ~30–35% killing in both of these normal cells (Fig. 5a and b). Acetazolamide functionalization of carbon dots made **CuCD-Az** more target specific towards TNBC, which resulted in ~2.8–3 fold higher cytotoxicity of **CuCD-Az** towards TNBC cells in comparison to HEK-293 and NIH3T3 cells. The scatterplot based on Annexin V-FITC/PI staining showed that in case of **CuCD-Az**, the majority of treated cells resided in the Q4 quadrant for MDA-MB-231 and 4T1, while for **CD-Az** they were mostly in the Q3 quadrant (Fig. S15). Thus, the cells underwent apoptosis through the early apoptotic pathway upon treatment with **CuCD-Az**. Furthermore, an intracellular GSH assay revealed that in the presence of **CD-Az** (3 mg mL^{-1}), almost no change in GSH concentration was observed in 4T1 and MDA-MB-231 when compared with untreated cells (Fig. S16). However, when the cells were treated with **CuCD-Az** (3 mg mL^{-1}), ~70% depletion of GSH concentration was observed in both cell lines (Fig. S16). Hence, there is depletion in intracellular GSH content in the presence of **CuCD-Az**. According to DCFH-DA staining, bright green fluorescence of 2′,7′-dichlorofluorescein (DCF) was observed in TNBC cells when treated with **CuCD-Az** (Fig. S17). In contrast, almost no green fluorescence was observed in **CD-Az**-treated cells (Fig. S17). Thus, DCFH-DA staining confirmed the significant amount of ROS generation by Cu^{+} ions inside cancer cells leading to apoptosis. Therefore, intracellular GSH assay and ROS generation study together confirmed the proposed CDT mechanism that intracellular GSH converted Cu^{2+} to Cu^{+} ions, which produced ROS upon reaction with intracellular H_2O_2.

In summary, we have developed CA-IX targeting acetazolamide-functionalized copper-doped (**CuCD-Az**) intrinsically fluorescent carbon dots, which showed considerable selectivity in the diagnosis of TNBC cells. **CuCD-Az** was capable of depleting GSH followed by ROS generation through Fenton-like reaction resulting in ~3 fold higher killing of cancer cells in comparison to normal cells. Thus, CA-IX targeting **CuCD-Az** has emerged as a potential theranostic probe for cancer cells *via* CDT.

A. H. K. and S. P. acknowledge CSIR, India and UGC, India for the respective research fellowships.

Conflicts of interest

There are no conflicts to declare.

Data availability

The data supporting this article have been included as part of the SI. Supplementary information: Experimental methods, synthetic scheme, table on literature survey, ^{13}C spectra, HRMS, AFM, fluorescence and XPS spectra of the carbon dots, EDX spectra of **CD-Az**, IR spectra, XRD spectra, raw data of western blots, bioimaging using **CD**, bioimaging after pre-treatment with acetazolamide, cytocompatibility, hemolytic assay, flow cytometric plots, intracellular GSH assay, and ROS generation using DCFH-DA staining. See DOI: **https://doi.org/10.1039/d5cc04653j**.

Notes and references

1 P. Kumar and R. Aggarwal, *Arch. Gynecol. Obstet.*, 2016, **293**, 247–269.
2 C. K. Kim, P. Ghosh, C. Pagliuca, Z. J. Zhu, S. Menichetti and V. M. Rotello, *J. Am. Chem. Soc.*, 2009, **131**, 1360–1361.
3 S. Brahmachari, D. Das, A. Shome and P. K. Das, *Angew. Chem., Int. Ed.*, 2011, **50**, 11243–11247.
4 J. Llop and T. Lammers, *ACS Nano*, 2021, **15**, 16794–16981.
5 S. Zhu, Q. Meng, L. Wang, J. Zhang, Y. Song, H. Jin, K. Zhang, H. Sun, H. Wang and B. Yang, *Angew. Chem., Int. Ed.*, 2013, **52**, 3953–3957.
6 M. Bartkowski, Y. Zhou, M. N. A. Mustafa, A. J. Eustace and S. Giordani, *Chem. – Eur. J.*, 2024, **30**, e202303982.
7 S. N. Baker and G. A. Baker, *Angew. Chem., Int. Ed.*, 2010, **49**, 6726–6744.
8 D. Chakraborty, S. Sarkar and P. K. Das, *ACS Sustainable Chem. Eng.*, 2018, **6**, 4661–4670.
9 A. B. Bourlinos, A. Stassinopoulos, D. Anglos, R. Zboril, M. Karakassides and E. P. Giannelis, *Small*, 2008, **4**, 455–458.
10 P. Zhao, H. Li and W. Bu, *Angew. Chem., Int. Ed.*, 2023, **62**, e202210415.
11 C. Chen, Y. Tan, T. Xu, Y. Sun, S. Zhao, Y. Ouyang, Y. Chen, L. He, X. Liu and H. Liu, *Langmuir*, 2022, **38**, 12307–12315.
12 Q. Li, J. Yu, L. Lin, Y. Zhu, Z. Wei, F. Wan, X. Zhang, F. He and L. Tian, *ACS Appl. Mater. Interfaces*, 2023, **15**, 16482–16491.
13 X. Cheng, H. D. Xu, H. H. Ran, G. Liang and F. G. Wu, *ACS Nano*, 2021, **15**, 8039–8068.
14 Y.-N. Hao, W.-X. Zhang, Y.-R. Gao, Y.-N. Wei, Y. Shu and J.-H. Wang, *J. Mater. Chem. B*, 2021, **9**, 250–266.
15 B. Ma, S. Wang, F. Liu, S. Zhang, J. Duan, Z. Li, Y. Kong, Y. Sang, H. Liu, W. Bu and L. Li, *J. Am. Chem. Soc.*, 2019, **141**, 849–857.
16 J. Li, A. Dirisala, Z. Ge, Y. Wang, W. Yin, W. Ke, K. Toh, J. Xie, Y. Matsumoto, Y. Anraku, K. Osada and K. Kataoka, *Angew. Chem., Int. Ed.*, 2017, **56**, 14025–14030.
17 W. Cao, J. Yang, C. Zhu, Z. Zeng, C. Yang, T. Chen and J. Zhu, *Bioconjugate Chem.*, 2023, **34**, 1166–1175.
18 J. Wang, Z. Sun, S. Wang, C. Zhao, J. Xu, S. Gao, M. Yang, F. Sheng, S. Gao and Y. Hou, *J. Am. Chem. Soc.*, 2022, **144**, 19884–19895.
19 W. Zuo, Z. Fan, L. Chen, J. Liu, Z. Wan, Z. Xioa, W. Chen, L. Wu, D. Chen and X. Zhu, *Acta Biomater.*, 2022, **147**, 258–269.
20 H. S. Jung, S. Koo, M. Won, S. An, H. Park, J. L. Sessler, J. Han and J. S. Kim, *Chem. Sci.*, 2023, **14**, 1808–1819.
21 N. Liu, Q. Lin, W. Zuo, W. Chen, S. Huang, Y. Han, X. J. Liang, X. Zhu and S. Huo, *Nanoscale Horiz.*, 2023, **8**, 783–793.
22 X. Chen, H. Zhang, M. Zhang, P. Zhao, R. Song, T. Gong, Y. Liu, X. He, K. Zhao and W. Bu, *Adv. Funct. Mater.*, 2020, **30**, 1908365.
23 A. M. Shabana, U. K. Mondal, M. R. Alam, T. Spoon, C. A. Ross, M. Madesh, C. T. Supuran and M. A. Ilies, *ACS Appl. Mater. Interfaces*, 2018, **10**, 17792–17808.
24 N. Krall, F. Pretto, W. Decurtins, G. J. L. Bernardes, C. T. Supuran and D. Neri, *Angew. Chem., Int. Ed.*, 2014, **53**, 4231–4235.
25 G. Biagiotti, A. Angeli, A. Giacomini, G. Toniolo, L. Landini, G. Salerno, L. D. C. Mannelli, C. Ghelardini, T. Mello, S. Mussi, C. Ravelli, M. Marelli, S. Cicchi, E. Menna, R. Ronca, C. T. Supuran and B. Richichi, *ACS Appl. Nano Mater.*, 2021, **4**, 14153–14160.
26 F. Yan, Z. Sun, J. Pang, Y. Jiang and W. Zheng, *Dyes Pigm.*, 2020, **183**, 108673.

